
Variational Control for Guidance in Diffusion Models

Kushagra Pandey^{*1,2} Farrin Marouf Sofian^{*1,2} Felix Draxler^{1,2} Theofanis Karaletsos³ Stephan Mandt^{1,4,2}

Abstract

Diffusion models exhibit excellent sample quality, but existing guidance methods often require additional model training or are limited to specific tasks. We revisit guidance in diffusion models from the perspective of variational inference and control, introducing *Diffusion Trajectory Matching* (DTM) that enables guiding pretrained diffusion trajectories to satisfy a terminal cost. DTM unifies a broad class of guidance methods and enables novel instantiations. We introduce a new method within this framework that achieves state-of-the-art results on several linear and (blind) non-linear inverse problems without requiring additional model training or modifications. For instance, in ImageNet non-linear deblurring, our model achieves an FID score of 34.31, significantly improving over the best pretrained-method baseline (FID 78.07). We will make the code available in a future update.

1. Introduction

Diffusion models (Sohl-Dickstein et al., 2015; Ho et al., 2020; Song et al., 2020) and related families (Lipman et al., 2023; Albergo & Vanden-Eijnden, 2023; Liu et al., 2023) exhibit excellent synthesis quality in large-scale generative modeling applications. Additionally, due to their principled design, these models exhibit great potential in serving as powerful generative priors for downstream tasks (Daras et al., 2024).

Consequently, guidance in diffusion models has received significant interest. However, the dominant approaches to classifier guidance (Dhariwal & Nichol, 2021) and classifier-free guidance (Ho & Salimans, 2021) require training additional models or retraining diffusion models for each conditioning task at hand, or are based on simplistic assumptions

detrimental to sample quality (Kawar et al., 2022; Chung et al., 2022a; Song et al., 2022b; Pandey et al., 2024b).

In this work, we generalize classifier guidance to a *variational control* problem (Kappen, 2008). Inspired by ideas such as *Control as Inference* (Kappen et al., 2012; Levine, 2018), we model guided diffusion dynamics as a Markov chain with the control signals defined as variational parameters. Variational inference is applied to optimize the control signals, ensuring that the process satisfies the desired terminal conditions while keeping the generated samples close to the unconditional sample manifold, see Fig. 1a. We denote this framework as *Diffusion Trajectory Matching* (DTM).

Recent work on steering diffusion models has already incorporated ideas from optimal control (Huang et al., 2024; Rout et al., 2024). However, these works focus on a restricted class of control problems. This obscures the available design choices revealed through our novel framework. Indeed, we find that DTM generalizes and explicitly contains a large class of prior work on guidance. We demonstrate the utility of this generalization by introducing a new sampling algorithm that seamlessly integrates with state-of-the-art diffusion model samplers like DDIM (Song et al., 2022a) and adapts well to diverse downstream tasks.

To summarize, we make the following contributions:

- We propose *Diffusion Trajectory Matching* (DTM), a generalized framework for training-free guidance based on a variational control perspective. DTM subsumes many existing and novel guidance methods.
- We instantiate our framework as *Non-linear Diffusion Trajectory Matching* (NDTM), which can be readily integrated with samplers like DDIM.
- NDTM outperforms previous state-of-the-art baselines for solving challenging noisy linear and (blind) non-linear inverse problems such as superresolution and inpainting with diffusion models (Daras et al., 2024) on FFHQ-256 (Karras et al., 2021) and ImageNet-256 (Deng et al., 2009).

2. Background

Diffusion Models. Given a perturbation kernel $p(\mathbf{x}_t|\mathbf{x}_0) = \mathcal{N}(\mu_t\mathbf{x}_0, \sigma_t^2\mathbf{I}_d)$, diffusion models (Sohl-Dickstein et al.,

^{*}Equal contribution ¹Department of Computer Science, University of California, Irvine ²AI Resident, Chan Zuckerberg Initiative, Redwood City, CA 94063 ³Chan Zuckerberg Initiative, Redwood City, CA 94063 ⁴Department of Statistics, University of California, Irvine. Correspondence to: Kushagra Pandey <pandeyk1@uci.edu>.

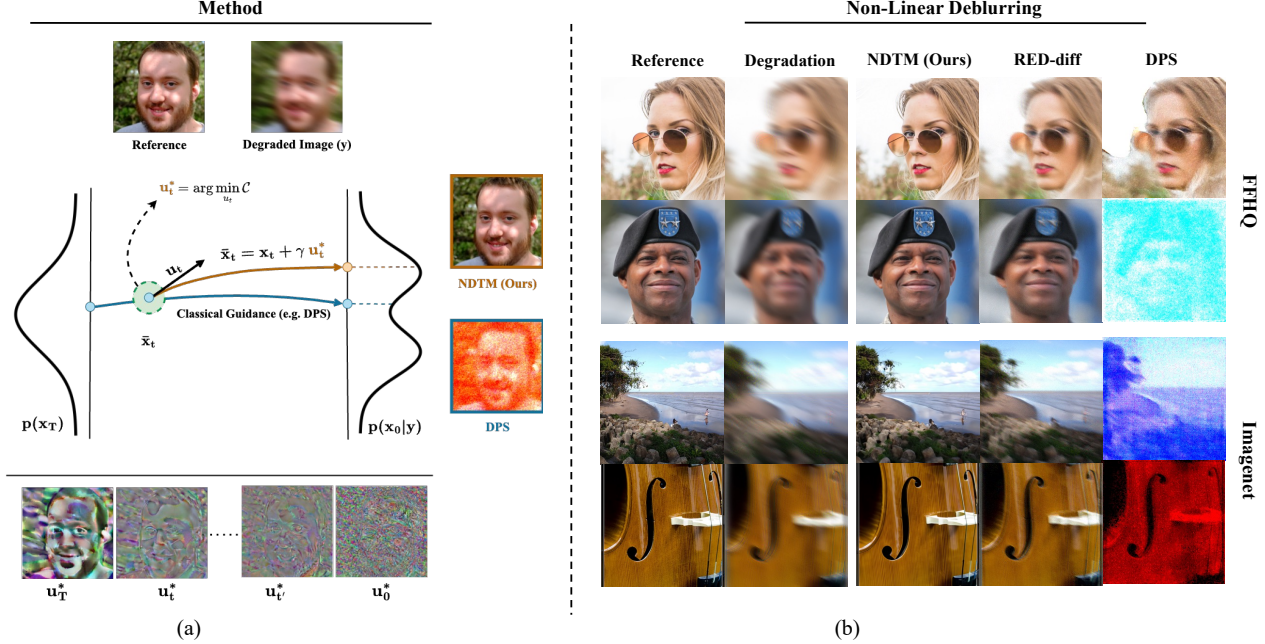


Figure 1. Our method guides diffusion sampling to fulfill external constraints. To this end, we optimize the local direction u_t^* via external constraints while respecting the original trajectory, see Eq. (11) (left, center). This recovers more accurate reconstructions across tasks compared to classical guidance methods: Nonlinear deblurring (Right). Our method accurately captures most details, while competing methods introduce artifacts in the generated reconstructions.

2015; Ho et al., 2020) invert the noising process by learning a corresponding reverse process parameterized as,

$$\mathcal{Q} : q(\mathbf{x}_{0:T-1} | \mathbf{x}_T) = \prod_t q(\mathbf{x}_{t-1} | \mathbf{x}_t). \quad (1)$$

The reverse diffusion posterior is specified as $q(\mathbf{x}_{t-1} | \mathbf{x}_t) = \mathcal{N}(\boldsymbol{\mu}_\theta(\mathbf{x}_t, t), \sigma_t^2 \mathbf{I}_d)$ where $\boldsymbol{\mu}_\theta(\cdot, \cdot)$ is learned via score matching (Hyvärinen & Dayan, 2005; Vincent, 2011; Song & Ermon, 2019). Analogously continuous-time diffusion models (Song et al., 2020; Karras et al., 2022) assume that a *forward process*

$$d\mathbf{x}_t = f(t)\mathbf{x}_t dt + g(t) d\mathbf{w}_t, \quad t \in [0, T], \quad (2)$$

with an drift $f(t)$ and diffusion coefficients $g(t)$ and standard Wiener process \mathbf{w}_t , converts data $\mathbf{x}_0 \in \mathbb{R}^d$ into noise \mathbf{x}_T . A *reverse* SDE specifies how data is generated from noise (Anderson, 1982; Song et al., 2020),

$$d\mathbf{x}_t = [f(t)\mathbf{x}_t - g(t)^2 \nabla_{\mathbf{x}_t} \log p_t(\mathbf{x}_t)] dt + g(t) d\bar{\mathbf{w}}_t, \quad (3)$$

which involves the *score* $\nabla_{\mathbf{x}_t} \log p_t(\mathbf{x}_t)$ of the marginal distribution over \mathbf{x}_t at time t . The score is intractable to compute and is approximated using a parametric estimator $s_\theta(\mathbf{x}_t, t)$, trained using denoising score matching.

Classifier Guidance in Diffusion Models. Given a pre-trained diffusion model $s_\theta(\mathbf{x}_t, t)$, it is often desirable to

guide the diffusion process conditioned on input \mathbf{y} . Consequently, the conditional diffusion dynamics read

$$d\mathbf{x}_t = [f(t)\mathbf{x}_t - g(t)^2 \nabla_{\mathbf{x}_t} \log p(\mathbf{x}_t | \mathbf{y})] dt + g(t) d\bar{\mathbf{w}}_t. \quad (4)$$

In classifier guidance (Dhariwal & Nichol, 2021), the conditional score can be decomposed as

$$\nabla_{\mathbf{x}_t} \log p(\mathbf{x}_t | \mathbf{y}) = s_\theta(\mathbf{x}_t, t) + \rho_t \nabla_{\mathbf{x}_t} \log p(\mathbf{y} | \mathbf{x}_t). \quad (5)$$

where ρ_t is the guidance weight. The noisy likelihood score is often estimated by training a noise-conditioned estimator. It is also common to estimate this likelihood via $p(\mathbf{y} | \mathbf{x}_t) = \int p(\mathbf{x}_0 | \mathbf{x}_t) p(\mathbf{y} | \mathbf{x}_0) d\mathbf{x}_0$. For example, Diffusion Posterior Sampling (DPS) (Chung et al., 2022a) approximates the diffusion posterior as, $p(\mathbf{x}_0 | \mathbf{x}_t) = \delta(\mathbb{E}[\mathbf{x}_0 | \mathbf{x}_t])$, where $\mathbb{E}[\mathbf{x}_0 | \mathbf{x}_t]$ is Tweedie’s estimate of the posterior at \mathbf{x}_t (Efron, 2011). This approximation of the diffusion posterior in DPS results in a high sampling budget and high sensitivity to the gradient weight ρ_t . More expressive approximations (Song et al., 2022b; Pandey et al., 2024b) result in specificity to linear inverse problems. We refer to Daras et al. (2024) for an in-depth discussion on explicit approximations of the diffusion posterior. We will show in Section 3.4 that classifier guidance in diffusion models is a special case of our proposed framework. Next, we discuss our proposed framework which can be directly applied to pretrained diffusion models and generalizes to linear and (blind) non-linear inverse problems.

3. Guidance with Diffusion Trajectory Matching (DTM)

We now propose a novel framework based on variational control for guidance in diffusion models. Our framework can be directly applied to pretrained diffusion models without requiring model retraining. For the remainder of our discussion, we restrict our attention to diffusion models and discuss an extension to flow-matching (Lipman et al., 2023) in Appendix A.3.

In the following, we first formulate guidance in discrete-time diffusion models as a variational optimal control problem (Section 3.1) following Kappen et al. (2012), which we refer to as *Diffusion Trajectory Matching* (DTM). We then present specific parameterizations of DTM in Section 3.2, which we work out as a guidance algorithm in Section 3.3. Lastly, in Appendix A.2, we transfer the DTM framework to continuous-time diffusion models (Song et al., 2020) and recover prior work in guidance in diffusion models.

3.1. Variational Control for Diffusion Guidance

The idea of our guidance framework is to take a controlled deviation from the *unguided diffusion trajectory* implied by Eq. (1) in Section 2, which we repeat for convenience:

$$\mathcal{Q} : q(\mathbf{x}_{0:T-1} | \mathbf{x}_T) = \prod_t q(\mathbf{x}_{t-1} | \mathbf{x}_t). \quad (6)$$

To steer the trajectory towards a target state fulfilling external constraints, we introduce a control signal \mathbf{u}_t at every time t . This yields the following *guided* dynamics for a given initial state \mathbf{x}_T :

$$\mathcal{P} : p(\mathbf{x}_{0:T-1} | \mathbf{x}_T, \mathbf{u}_{1:T}) = \prod_t p(\mathbf{x}_{t-1} | \mathbf{x}_t, \mathbf{u}_t). \quad (7)$$

While we model the guided dynamics as Markovian due to convenience, non-Markovian approximations are also possible (Li et al., 2021). Given a set of external constraints, the task is to determine the variational control \mathbf{u}_t . Consequently, following Kappen et al. (2012), we can pose this problem as a stochastic optimal control problem with the terminal and transient costs formulated as,

$$\mathcal{C}(\mathbf{x}_T, \mathbf{u}_{1:T}) = w_T \underbrace{\mathbb{E}_{\mathbf{x}_0 \sim p}[\Phi(\mathbf{x}_0)]}_{\text{Terminal Cost } \mathcal{C}_{\text{te}}} + \underbrace{D_{\text{KL}}(\mathcal{P} \parallel \mathcal{Q})}_{\text{Transient Cost } \mathcal{C}_{\text{tr}}}. \quad (8)$$

The terminal cost in Eq. (8) encodes desirable constraints on the final guided state while the transient cost ensures that the guided trajectory does not deviate strongly from the unguided trajectory, so that the final guided state \mathbf{x}_0 lies near the image manifold. The two losses are traded by a scalar w_T .

Choice of Terminal Cost. The terminal cost in Eq. (8) encodes desirable constraints on the final guided state. For instance, $\Phi(\mathbf{x}_0) \propto -\log p(\mathbf{y} | \mathbf{x}_0)$ could be the log-likelihood

of a probabilistic classifier for class-conditional generation or the degradation process for solving inverse problems. For instance, Huang et al. (2024) adapt guidance for a non-differentiable terminal cost using a path integral control (Kappen, 2005) formulation. While an interesting direction for further work, we only assume that the terminal cost is differentiable for now.

Choice of Divergence. We use the KL-Divergence as it decomposes over individual timesteps,

$$\mathcal{C}_{\text{tr}} = \sum_t \mathbb{E}_{\mathbf{x}_t} [D_{\text{KL}}(p(\mathbf{x}_{t-1} | \mathbf{x}_t, \mathbf{u}_t) \parallel q(\mathbf{x}_{t-1} | \mathbf{x}_t))]. \quad (9)$$

Note that other divergence measures can be useful depending on the specific form of the diffusion posterior (Nachmani et al., 2021; Zhou et al., 2023; Pandey et al., 2024a; Holderrieth et al., 2024).

Simplifications. The proposed loss in Eq. (8) is generic and principled, but is difficult to jointly optimize for all controls $\mathbf{u}_{1:T}$ due to the need to backpropagate through the entire diffusion trajectory. To avoid this computational overhead, we make several simplifications that make the objective computationally tractable. We justify the validity of the modifications through our empirical results in Section 4.

First, we optimize \mathbf{u}_t in a greedy manner, that is at any time t in the diffusion process we optimize \mathbf{u}_t , assuming that the remaining steps $t-1, \dots, 1$ are unguided. After optimizing for \mathbf{u}_t , we sample from the optimized posterior $\mathbf{x}_{t-1} \sim p(\mathbf{x}_{t-1} | \mathbf{x}_t, \mathbf{u}_t^*)$ and iterate. When the variational control of \mathbf{u}_t is flexible enough, suboptimal greedy choices early in the trajectory can be compensated for later.

Second, we evaluate the terminal cost at the current *expected* final guided state via Tweedie’s Formula for $\mathbb{E}[\mathbf{x}_0 | \mathbf{x}_t, \mathbf{u}_t]$:

$$\mathcal{C}_{\text{te}} = \mathbb{E}_{\mathbf{x}_0} [\Phi(\mathbf{x}_0)] \approx \Phi(\mathbb{E}[\mathbf{x}_0 | \mathbf{x}_t, \mathbf{u}_t]) = \Phi(\hat{\mathbf{x}}_0^t) \quad (10)$$

where we have approximated $p(\mathbf{x}_0 | \mathbf{x}_t, \mathbf{u}_t) \approx \delta(\mathbf{x}_0 - \hat{\mathbf{x}}_0^t)$.

Diffusion Trajectory Matching (DTM). Together, the optimization problem to solve at time t given a position \mathbf{x}_t reads:

$$\mathcal{C}(\mathbf{u}_t) = w_T \Phi(\hat{\mathbf{x}}_0^t) + D_{\text{KL}}(p(\mathbf{x}_{t-1} | \mathbf{x}_t, \mathbf{u}_t) \parallel q(\mathbf{x}_{t-1} | \mathbf{x}_t)). \quad (11)$$

We refer to Eq. (11) as *Diffusion Trajectory Matching* (DTM).

Continuous-Time Variants. To apply DTM to continuous-time diffusion and flow matching, we adapt the transient costs \mathcal{C}_{tr} . We call the following *Continuous-Time Diffusion Trajectory Matching* (CT-DTM), derived for continuous-time diffusion (Song et al., 2020) in Appendix A.2:

$$\mathcal{C}_{\text{tr}} = \frac{g(t)^2}{2} \mathbb{E}_{\mathbf{x}_t} \left[\left\| \mathbf{s}_{\theta}(\mathbf{x}_t, t) - \mathbf{s}_{\theta}(\mathbf{x}_t, \mathbf{u}_t, t) \right\|_2^2 \right]. \quad (12)$$

Algorithm 1 NDTM (DDIM). Sampling proceeds by inferring the control (shaded) followed by sampling from the guided posterior (shaded) at any time t

```

1: Input: Optimization Steps:  $N$ , Guidance:  $\gamma$ , Pretrained
   denoiser:  $\epsilon_\theta(\cdot, \cdot)$ , Timestep schedule:  $\{t\}_{j=0}^T$ , DDIM
   Coefficients:  $\alpha_t, \sigma_t$ , Loss Weights:  $\tau_t, \kappa_t, w_T$ 
2: Initialization:  $\mathbf{x}_T \sim \mathcal{N}(0, \mathbf{I}_d)$ 
3: for  $t = T$  to 1 do
4:    $\mathbf{u}_t^{(0)} = 0$ 
5:    $\hat{\mathbf{e}}_{\text{uncond}} \leftarrow \epsilon_\theta(\mathbf{x}_t, t)$ 
6:   for  $i = 0$  to  $N - 1$  do
7:      $\hat{\mathbf{e}}_{\text{control}}^{(i)} \leftarrow \epsilon_\theta(\mathbf{x}_t + \gamma \mathbf{u}_t^{(i)}, t)$ 
8:      $\hat{\mathbf{x}}_0^{(i)} \leftarrow \mathbb{E}[\mathbf{x}_0 | \mathbf{x}_t + \gamma \mathbf{u}_t^{(i)}]$ 
9:      $C_{\text{score}} = \tau_t^2 \left\| \hat{\mathbf{e}}_{\text{uncond}} - \hat{\mathbf{e}}_{\text{control}}^{(i)} \right\|_2^2$ 
10:     $C_{\text{control}} = \kappa_t^2 \|\mathbf{u}_t\|_2^2$ 
11:     $C_{\text{terminal}} = w_T \Phi(\hat{\mathbf{x}}_0^{(i)})$ 
12:     $C_t^{(i)} \leftarrow C_{\text{score}} + C_{\text{control}} + C_{\text{terminal}}$ 
13:     $\mathbf{u}_t^{(i+1)} \leftarrow \text{Update}(\mathbf{u}_t^{(i)}, \nabla_{\mathbf{u}_t} C_t^{(i)})$ 
14:  end for
15:   $\mathbf{x}_{t-1} \leftarrow \text{DDIM}(\mathbf{x}_t + \gamma \mathbf{u}_t^*, t)$ 
16: end for
17: return  $\mathbf{x}_0$ 
    
```

Similarly, for flow matching (Lipman et al., 2023; Liu et al., 2023; Albergo et al., 2023), we refer to this as *Flow Trajectory Matching* (FTM), see Appendix A.3:

$$C_{\text{tr}} = \|\mathbf{v}_\theta(\mathbf{x}_t, t) - \mathbf{v}_\theta(\mathbf{x}_t, \mathbf{u}_t, t)\|^2. \quad (13)$$

Next, we present a specific parameterization of our framework and its instantiation using standard diffusion models.

3.2. Non-linear Diffusion Trajectory Matching (NDTM)

In the context of Gaussian diffusion models (Ho et al., 2020; Song et al., 2020; Karras et al., 2022), the unguided diffusion posterior is often parameterized as,

$$q(\mathbf{x}_{t-1} | \mathbf{x}_t) = \mathcal{N}(\boldsymbol{\mu}_\theta(\mathbf{x}_t, t), \sigma_t^2 \mathbf{I}_d) \quad (14)$$

For the guided diffusion posterior, we choose the following parameterization such that the control can affect the diffusion dynamics non-linearly.

$$p(\mathbf{x}_{t-1} | \mathbf{x}_t, \mathbf{u}_t) = \mathcal{N}(\boldsymbol{\mu}_\theta(\mathbf{x}_t, \mathbf{u}_t, t), \sigma_t^2 \mathbf{I}_d). \quad (15)$$

From a practical standpoint, since unconditional score models are usually parameterized using neural networks with an input noisy state and a timestep embedding, we further parameterize the posterior mean $\boldsymbol{\mu}_\theta(\mathbf{x}_t, \mathbf{u}_t, t) = \boldsymbol{\mu}_\theta(\mathbf{f}(\mathbf{x}_t, \mathbf{u}_t, t), t)$, where the *aggregation* function \mathbf{f} :

$\mathbb{R}^d \times \mathbb{R}^d \times \mathbb{R} \rightarrow \mathbb{R}^d$ combines the noisy state \mathbf{x}_t and the control \mathbf{u}_t appropriately. In this work, we choose an additive form of $\mathbf{f} = \mathbf{x}_t + \gamma \mathbf{u}_t$ where γ is the *guidance weight* used to update the current noisy state \mathbf{x}_t in the direction of the control signal \mathbf{u}_t . We leave exploring other aggregation functions as future work. Moreover, in practice, we sample from a single diffusion trajectory and therefore omit the expectation in Eq. (11). Consequently, the control cost in Eq. (11) can be simplified as,

$$\mathcal{C}(\mathbf{u}_t) = \|\boldsymbol{\mu}_\theta(\mathbf{x}_t + \gamma \mathbf{u}_t, t) - \boldsymbol{\mu}_\theta(\mathbf{x}_t, t)\|_2^2 + w_T \Phi(\hat{\mathbf{x}}_0^t). \quad (16)$$

Due to the non-linear dependence of the guided posterior on the control signal \mathbf{u}_t , we refer to the transient cost specification in Eq. 16 as *Non-Linear Diffusion Trajectory Matching* (NDTM). We will show in Section 3.4 that linear control can be formulated as a special case of this parameterization, yielding classifier guidance. Next, we instantiate the NDTM objective practically.

3.3. Specific Instantiations

Here, we present a simplified form of the NDTM objective in the context of DDIM (Song et al., 2022a).

Proposition 3.1. *For the diffusion posterior parameterization in DDIM (Song et al., 2022a), the NDTM objective in Eq. 16 has the following tractable upper bound (see proof in Appendix A.1),*

$$\mathcal{C}(\mathbf{u}_t) \leq \kappa_t^2 \|\mathbf{u}_t\|_2^2 + \tau_t^2 \|\epsilon_\theta(\bar{\mathbf{x}}_t, t) - \epsilon_\theta(\mathbf{x}_t, t)\|_2^2 + w_T \Phi(\hat{\mathbf{x}}_0^t), \quad (17)$$

where $\bar{\mathbf{x}}_t = \mathbf{x}_t + \gamma \mathbf{u}_t$ is the guided state and the coefficients $\kappa_t = \frac{\gamma \sqrt{\alpha_{t-1}}}{\sqrt{\alpha_t}}$ and $\tau_t = \sqrt{1 - \alpha_{t-1} - \sigma_t^2} - \frac{\sqrt{\alpha_{t-1}(1-\alpha_t)}}{\sqrt{\alpha_t}}$ are time-dependent scalars.

The coefficients α_t and σ_t are specific to DDIM (see Appendix A.1 for more details). Intuitively, the simplified NDTM loss in Eq. (17) measures the deviation between the guided and unguided dynamics, penalizing the magnitude of the control signal \mathbf{u}_t (first term) and deviations in the noise predictions (second term). On the contrary, the terminal loss ensures that the *expected* final guided state satisfies the external constraints. Therefore, the first two terms in Eq. (17) act as regularizers on the control signal \mathbf{u}_t .

In Appendix A.2, we derive this simplification also for continuous-time diffusion models.

Putting it all together. To summarize, at each diffusion time step t , we estimate the control signal \mathbf{u}_t by minimizing the cost $\mathcal{C}(\mathbf{u}_t)$ (for instance Eq. (17) for DDIM). This iterative optimization allows the model to dynamically adjust the control to best align the trajectory with the desired terminal cost while minimizing deviations with the unguided

diffusion trajectory. Finally, we sample from the guided posterior $p(\mathbf{x}_{t-1}|\mathbf{x}_t, \mathbf{u}_t^*)$. We provide a visual illustration of the NDTM algorithm in Fig. 1a and its pseudocode implementation in Algorithm 1.

3.4. Connection to Existing Guidance Mechanisms

In this section, we rigorously establish a connection between optimal control and classifier guidance: Our variational formulation in Section 3.1 captures existing approaches. We derive this result in the continuous-time variant, as this allows for a closed-form solution of the control problem.

In particular, let us choose a linear parameterization of the guided score in Eq. (12), that is $s_\theta(\mathbf{x}_t, \mathbf{u}_t, t) = s_\theta(\mathbf{x}_t, t) + \mathbf{u}_t$. Then, the transient cost reduces to:

$$C_{\text{tr}} = \int \|\mathbf{u}_t\|^2 dt. \quad (18)$$

This is exactly the case of the well-established *Path Integral Control* (Kappen, 2005; 2008). The solution of this optimal control problem in Eq. (8) reads (Kappen, 2008, Eq. (34)):

$$\mathbf{u}_t^* = g(t)w_T \nabla_{\mathbf{x}_t} \log \mathbb{E}_{p(\mathbf{x}_0|\mathbf{x}_t)}[\exp(-\Phi(\mathbf{x}_0))]. \quad (19)$$

Notably, if the terminal cost takes the form of a classifier likelihood $\Phi(\mathbf{x}_0) \propto -\log p(\mathbf{y}|\mathbf{x}_0)$, it can be shown (Huang et al., 2024) that the optimal control simplifies to classifier guidance (Dhariwal & Nichol, 2021): $\mathbf{u}_t^* = g(t)w_T \nabla_{\mathbf{x}_t} p(\mathbf{y}|\mathbf{x}_t)$.

This puts a large class of methods approximating the expectation over the posterior $p(\mathbf{x}_0|\mathbf{x}_t)$ (Chung et al., 2022a; Song et al., 2022b; Pandey et al., 2024b; Huang et al., 2024) into perspective: In terms of our DTM framework, they perform optimal control with a linear control mechanism. Empirically, we will see in Section 4 that our generalization to non-linear control provides significant performance improvements.

4. Experiments

While our method serves as a general framework for guidance in diffusion models, here, we focus on solving inverse problems (IP). Through both quantitative and qualitative results, we demonstrate that our approach outperforms recent state-of-the-art baselines across various (blind) non-linear and linear inverse problems. Lastly, we emphasize key design parameters of our proposed method as ablations. We present full implementation details in Appendix B.

Problem Setup Given a corruption model \mathcal{A} and a noisy measurement $\mathbf{y} \in \mathbb{R}^d$ the goal is to recover the unknown sample $\mathbf{x}_0 \sim p_{\text{data}}$, from the degradation $\mathbf{y} = \mathcal{A}(\mathbf{x}_0) + \sigma_y \mathbf{z}$, $\mathbf{z} \sim \mathcal{N}(\mathbf{0}, \mathbf{I}_d)$. For linear inverse problems, $\mathbf{y} = \mathbf{A}\mathbf{x}_0$ where \mathbf{A} can be any matrix. In the case where only the

functional form of the degradation operator \mathcal{A} is known but its parameters are not, the problem is known as Blind IP.

Models and Datasets: We conduct experiments on the FFHQ (256×256) (Karras, 2019) and ImageNet (256×256) (Deng et al., 2009) datasets, using a held-out validation set of 1,000 samples from each. For FFHQ, we use the pre-trained model provided by Chung et al. (2022a), and for ImageNet, we use the unconditional pre-trained checkpoint from OpenAI (Dhariwal & Nichol, 2021).

Tasks and Metrics: We consider two linear and two non-linear inverse problems with noise level $\sigma_y = 0.01$. For linear inverse problems, we use inpainting and super-resolution. For non-linear problems, we perform non-linear deblurring and blind image deblurring (BID) (see Appendix B).

To quantitatively evaluate our results, we report metrics optimized for perceptual quality, including Learned Perceptual Image Patch Similarity (LPIPS) (Zhang et al., 2018b), Fréchet Inception Distance (FID) (Heusel et al., 2017), and Kernel Inception Distance (KID) (Bińkowski et al., 2018). For completeness, recovery metrics like the Peak Signal-to-Noise Ratio (PSNR) are provided in Appendix C. With the exception of BID (for which we use 100 images), we evaluate all other inverse problems on 1k images.

Baselines For linear tasks, we compare our proposed method against several state-of-the-art approaches, namely DPS (Chung et al., 2022a), RED-diff (Mardani et al., 2023b), C-IIGDM (Pandey et al., 2024b), and DDRM (Kawar et al., 2022). Since the latter two are restricted to linear degradation settings, for non-linear deblurring, we only compare our method with DPS and RED-diff. We also consider a recently proposed method, DMPlug (Wang et al., 2024), as a potential baseline. However, we find that DMPlug is too computationally expensive to evaluate on 1k samples (see Appendix C for details on runtimes). Therefore, we only use this baseline for the BID task evaluated on 100 images from the FFHQ dataset since, to the best of our knowledge, it is currently state-of-the-art in this task.

Sampling Setup. We tune all samplers for the best perceptual quality. We highlight sampler parameters that are common across all tasks and discuss task-specific sampler configs in the Appendix B.

- **DPS:** We adapt the tuned hyperparameters for DPS from (Mardani et al., 2023b). More specifically, we set DDIM $\eta = 0.5$, number of sampling steps to 1000.
- **RED-diff:** We set $\sigma_0 = 0$ with a linear weighting schedule and $lr = 0.5$ and perform 50 diffusion steps. We tune λ depending on the task.
- **DDRM:** We fix $\eta = 0.85$, $\eta_b = 1.0$, and the number of diffusion steps to 20 across all linear IPs.

Table 1. Comparisons on **noisy Non-linear Deblur**. NDTM outperforms competing baselines by a significant margin. **Bold**: best.

Method	FFHQ (256 × 256)			ImageNet (256 × 256)		
	LPIPS↓	FID↓	KID↓	LPIPS↓	FID↓	KID↓
DPS	0.752	249.01	0.139	0.888	346.82	0.2186
RED-diff	0.362	64.57	0.0363	0.416	78.07	0.0224
NDTM (ours)	0.046	14.198	0.0004	0.163	34.31	0.0032

- **C-IIGDM**: We set the number of diffusion steps to 20 since C-IIGDM (Pandey et al., 2024b) saturates in performance within this budget. Furthermore, since Pandey et al. (2024b) report performance on noiseless inverse problems, we re-tune C-IIGDM for best perceptual quality (with $\sigma_y = 0.01$) on all tasks and provide detailed hyperparameters in the Appendix.
- **DMPlug**: Following (Wang et al., 2024), we fix diffusion steps to 3, number of optimization steps to 10k, and the (kernel, method) learning rates to (0.01, 0.1).
- **(Ours) NDTM**: We fix the learning rate for the control, \mathbf{u}_t , to 0.01 across all tasks and apply a linear decay schedule over optimization steps. We tune the guidance weight γ , loss weighting, and DDIM η for best performance across different tasks. We choose the number of optimization steps N based on a tradeoff between sample quality and compute.

4.1. Non-linear Inverse Problems

Non-Linear Deblurring. As a first non-linear IP, we consider non-linear deblurring with the same setup as in Chung et al. (2022a). Figure 2 (Left) illustrates the comparison between competing baselines and our proposed method, NDTM, on this task. Qualitatively, similar to Mardani et al. (2023a), we find that DPS is very sensitive to guidance step size and is usually unstable on this task. Moreover, while RED-diff does not have stability issues, we find that it is biased towards generating blurry samples. This is not surprising given their unimodal approximation to the data posterior $p(\mathbf{x}_0|y)$. On the contrary, NDTM generates high-fidelity reconstructions with a stable sampling process. Similarly, our quantitative results in Table 1 validate our qualitative findings as our method outperforms competing baselines on perceptual quality for both datasets by a significant margin.

Blind Image Deblurring (BID). Next, we extend our framework to blind image deblurring, maintaining the same setup as DMPlug (Wang et al., 2024), which is the state-of-the-art method for this task. Interestingly, adapting our proposed method for blind inverse problems involves jointly optimizing the unknown blur kernel parameters along with the control \mathbf{u}_t . More specifically, for degradation of the form $y = k * \mathbf{x}_0 + \sigma_y z$ with unknown blurring kernel k , we

Table 2. Comparisons on **noisy Blind Image Deblurring (BID)** for the FFHQ 256×256 dataset. NDTM outperforms DMPlug (Wang et al., 2024) by a significant margin while requiring an order of magnitude less sampling time (reported in minutes/img). **Bold**: best. †: N=15, T=200, ‡: N=15, T=400.

Method	Gaussian blur			Motion blur		
	LPIPS↓	FID↓	Time↓	LPIPS↓	FID↓	Time↓
DMPlug	0.147	69.36	51.24	0.118	72.85	51.13
NDTM† (Ours)	0.103	55.15	7.17	0.086	49.99	7.17
NDTM‡ (Ours)	0.083	47.34	18.07	0.063	38.6	18.13

update line 11 in Algorithm 1 as $\mathcal{C}_{\text{terminal}} = w_T \Phi(\hat{\mathbf{x}}_0^{(i)}, k^{(i)})$ and optimizing for the trainable kernel for each image, as $k^{(i+1)} \leftarrow \text{Update}(k^{(i)}, \nabla_k \mathcal{C}_t^{(i)})$.

Figure 2 (Right) illustrates the comparison between DMPlug and NDTM adapted for this task. Qualitatively, we find that while DMPlug can introduce artifacts in generating reconstructions, NDTM generates high-quality reconstructions. Table 2 further validates our qualitative findings as our method outperforms DMPlug on perceptual quality metrics. More interestingly, while DMPlug is extremely expensive for a single image, our method outperforms the former on sample quality by a significant margin while being an order of magnitude faster. This illustrates that our sampler has a more efficient way to trade sampling speed for quality. We additionally present quantitative results for a more efficient configuration ($N = 15, T = 200$) of our proposed method that maintains strong performance in Table 2, with corresponding qualitative results provided in Appendix C.

4.2. Linear Inverse Problems

Lastly, we compare competing methods on linear inverse problems: (4x) Super-resolution and Random inpainting with a 90% masking probability. As illustrated in Table 3, for super-resolution, NDTM outperforms competing baselines for both datasets. For random inpainting, our method performs comparably with DPS on the FFHQ dataset. However, for a more difficult benchmark like ImageNet, NDTM outperforms the next best-competing baseline, DPS on this task. We present additional qualitative results for linear inverse problems in Appendix C

4.3. Ablation Studies

Next, we analyze the impact of different design choices in NDTM on the perception (LPIPS) and distortion (PSNR) quality for the non-linear deblur task on the ImageNet dataset.

Impact of Guidance. Since the terminal cost weight w_T and the parameter γ affect the optimization of the variational control parameters \mathbf{u}_t , we analyze their impact on

Table 3. NDTM performs on-par/better than competing baselines on noisy linear inverse problems. Missing entries indicate unstable performance after multiple tuning attempts **Bold**: best.

Method	Super-Resolution (4x)						Random Inpainting (90%)					
	FFHQ (256 × 256)			Imagenet (256 × 256)			FFHQ (256 × 256)			Imagenet (256 × 256)		
	LPIPS↓	FID↓	KID↓	LPIPS↓	FID↓	KID↓	LPIPS↓	FID↓	KID↓	LPIPS↓	FID↓	KID↓
DPS	0.061	20.61	0.0029	0.195	30.67	0.0021	0.058	20.24	0.0019	0.152	32.56	0.0023
DDRM	0.116	36.13	0.0183	0.325	52.76	0.0151	0.582	167.57	0.1530	0.791	211.66	0.1517
RED-diff	0.151	41.54	0.0179	0.354	51.83	0.0084	0.430	155.49	0.1370	0.633	218.88	0.1531
C-IIGDM	0.106	29.61	0.0073	0.270	39.96	0.0024	0.551	137.85	0.1020	-	-	-
NDTM (ours)	0.054	18.99	0.0019	0.158	28.75	0.0011	0.059	20.11	0.0020	0.149	30.43	0.0018

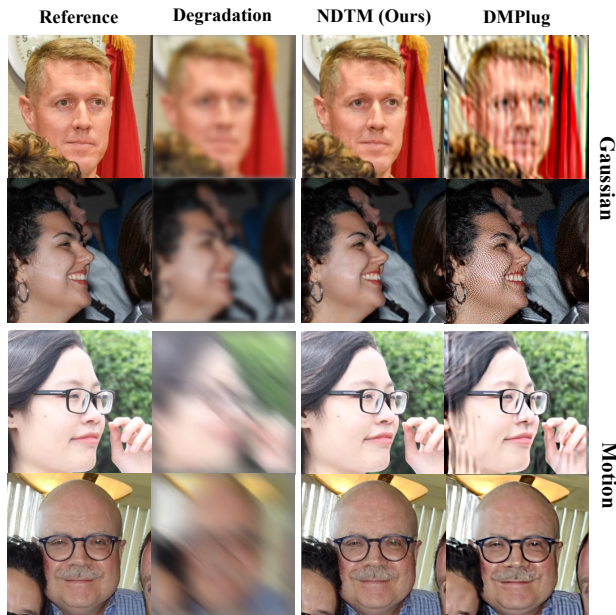


Figure 2. NDTM outperforms competing baselines on noisy blind image deblurring (BID) with Gaussian (top) and Motion (bottom) kernels. NDTM accurately captures most details, while competing methods introduce artifacts in the generated reconstructions.

sample quality. From Fig. 3a, we observe that increasing the terminal weight w_T leads to an improvement in both perceptual and distortion quality. However, in the limit of $w_T \rightarrow \infty$ (i.e., where the regularization terms in Eq. 17 can be ignored), the perceptual quality degrades, which highlights the importance of the transient cost in our framework. Similarly, increasing γ also leads to an improved sample quality. However, a large γ can also lead to overshooting which can lead to a degradation in sample quality.

Impact of Optimization Steps. It is common to trade sample quality for the number of sampling steps in diffusion models. Interestingly, NDTM provides a complementary axis to achieve this tradeoff in the form of adjusting the number of optimization steps per diffusion update. We illus-

trate this in Fig. 3(b), where for a fixed sampling budget of 50 diffusion steps, NDTM can achieve better reconstruction quality by increasing the number of optimization steps (N). However, since the runtime increases linearly as N grows (see Figure 3(d)), a practical choice depends on the available compute. We find that for this task, $N=2$ provides a favorable tradeoff between sampling time and quality and, therefore, use it for state-of-the-art comparisons on the ImageNet dataset in Table 1.

Control Visualizations We visualize the optimal controls \mathbf{u}_t^* in Figure 4. We observe a hierarchical refinement of image features over time. More specifically, the control inference captures global structure at the start of diffusion sampling and gradually refines local details (like edges), thereby encoding high-frequency information at later steps.

5. Related Work

Conditional Diffusion Models. In general, the conditional score $\nabla_{\mathbf{x}_t} \log p(\mathbf{x}_t | \mathbf{y})$ needed for guided sampling can be learned during training (Saharia et al., 2022; Podell et al., 2024; Rombach et al., 2022) or approximated during inference. Here, we focus on training-free guidance during inference.

In this context, there has been some recent progress in approximating the noisy likelihood score (see Eq. 5) by approximating the diffusion posterior $p(\mathbf{x}_0 | \mathbf{x}_t)$. For instance, DPS (Chung et al., 2022a) approximates the diffusion posterior by a Dirac distribution centered on Tweedie’s estimate (Efron, 2011). This has the advantage that the guidance can be adapted to linear and non-linear tasks alike. However, due to a crude approximation, DPS converges very slowly and, in our observation, could be unstable for certain tasks (see Table 1). Consequently, some recent work (Yu et al., 2023; Bansal et al., 2024) adds a correction term on top of the DPS update rule to better satisfy the constraints. In addition to being more principled, our proposed method instead directly estimates the guided posterior at each sampling step, thus sidestepping the limitations of DPS in the first place.

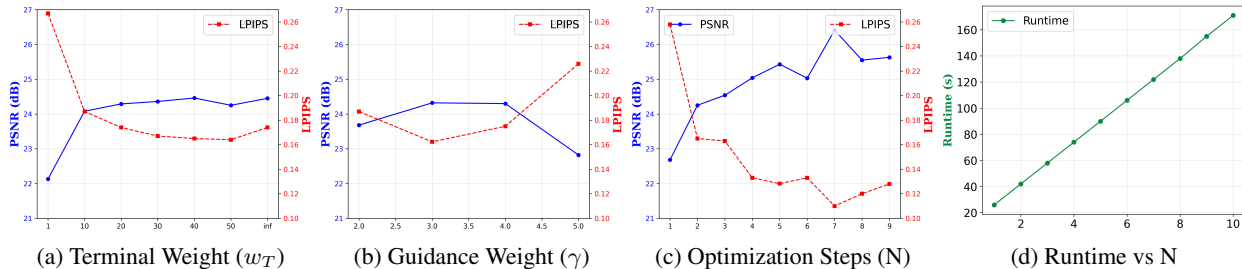


Figure 3. **Impact of different design choices** in NDTM on Distortion (PSNR) and Perception (LPIPS) for the non-linear deblur task. (a, b) The extent of guidance can be jointly controlled by varying the terminal loss weight (w_T) and the weight (γ). (c, d) Compute vs quality can be traded off by jointly varying the number of optimization steps (N) and the number of diffusion steps.

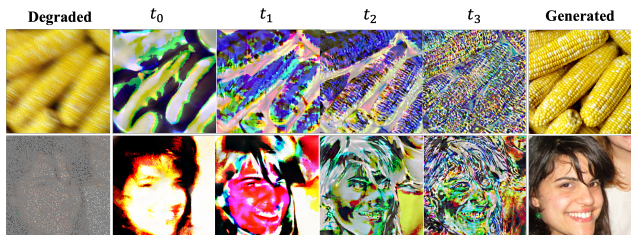


Figure 4. **The optimal variational controls hierarchically refine image features over time.** (Top Row) Non-Linear Deblur (Bottom Row) Random Inpainting. (Left to Right) We visualize optimal controls at different times $t_0 > t_1 > t_2 > t_3$ in diffusion sampling, progressively capturing coarse to fine details.

More recent work (Song et al., 2022b; Pandey et al., 2024b; Pogle et al., 2024; Boys et al., 2023) relies on expressive approximations of the diffusion posterior. While this can result in accurate guidance and faster sampling, a large proportion of these methods are limited to linear inverse problems. In contrast, our method can be adapted to generic inverse problems with some additional computational overhead. Lastly, another line of work in inverse problems approximates the data posterior $p(\mathbf{x}_0|\mathbf{y})$ using variational inference (Zhang et al., 2018a). For instance, RED-diff (Mardani et al., 2023a) proposes to learn a unimodal approximation to the data posterior by leveraging a diffusion prior. However, this can be too restrictive in practice and comes at the expense of blurry samples. We refer interested readers to Daras et al. (2024) for a more detailed review of training-free methods for solving inverse problems in diffusion models.

Optimal Control for Diffusion Models. There has been some recent interest in exploring connections between stochastic optimal control and diffusion models (Berner et al., 2024). Chen et al. (2024) leverage ideas from control theory for designing efficient diffusion models with straight-line trajectories in augmented spaces. Since our guided sampler can be used with any pretrained diffusion models, our approach is complementary to this line of work.

More recently, SCG (Huang et al., 2024) leverages ideas from path integral control to design guidance schemes with non-differentiable constraints. In contrast, we only focus on differentiable terminal costs, and extending our framework to non-differentiable costs could be an important direction for future work. Lastly, Rout et al. (2024) propose RB-Modulation, a method based on control theory for personalization using diffusion models. Interestingly, while RB-Modulation is primarily inspired by a class of tractable problems in control theory, it is a special case of our framework in the limit of $w \rightarrow \infty$ and $\gamma = 1$. Therefore, our proposed framework is more flexible.

6. Conclusion

Our novel framework elucidates the design space of guidance in diffusion models. Through the lens of variational optimal control, it offers a principled way to guide a pre-trained diffusion model while respecting an external cost. Our empirical results suggest that optimizing each diffusion step allows for more flexibility in guidance compared to commonly used approximations of the diffusion posterior.

While our method adapts well to linear and (blind) non-linear problems, there remain several interesting directions for future work. First, a more thorough theoretical investigation into the optimization dynamics of the proposed method could help alleviate the extra overhead of variational inference during each diffusion sampling. Second, it would be interesting to extend our method to Latent Diffusion Models (LDMs) (Rombach et al., 2022). Lastly, our method is only one instantiation of our framework, leaving ample room for exploration. Investigating variational parameterizations, refining cost functions, and developing more efficient optimization schemes could further enhance the flexibility and applicability of our approach.

Acknowledgment. We thank Justus Will for additional discussions and feedback. This project was funded through support from the Chan Zuckerberg Initiative. Addition-

ally, Stephan Mandt acknowledges funding from the National Science Foundation (NSF) through an NSF CAREER Award IIS-2047418, IIS-2007719, the NSF LEAP Center, the IARPA WRIVA program, and the Hasso Plattner Research Center at UCI.

References

- Albergo, M. and Vanden-Eijnden, E. Building normalizing flows with stochastic interpolants. In *ICLR 2023 Conference*, 2023.
- Albergo, M. S., Boffi, N. M., and Vanden-Eijnden, E. Stochastic interpolants: A unifying framework for flows and diffusions. *arXiv preprint arXiv:2303.08797*, 2023.
- Anderson, B. D. Reverse-time diffusion equation models. *Stochastic Processes and their Applications*, 12(3):313–326, 1982. ISSN 0304-4149. doi: [https://doi.org/10.1016/0304-4149\(82\)90051-5](https://doi.org/10.1016/0304-4149(82)90051-5). URL <https://www.sciencedirect.com/science/article/pii/0304414982900515>.
- Bansal, A., Chu, H.-M., Schwarzschild, A., Sengupta, R., Goldblum, M., Geiping, J., and Goldstein, T. Universal guidance for diffusion models. In *The Twelfth International Conference on Learning Representations*, 2024. URL <https://openreview.net/forum?id=pzpwBbnwiJ>.
- Berner, J., Richter, L., and Ullrich, K. An optimal control perspective on diffusion-based generative modeling. *Transactions on Machine Learning Research*, 2024. ISSN 2835-8856. URL <https://openreview.net/forum?id=oYIjw37pTP>.
- Bińkowski, M., Sutherland, D. J., Arbel, M., and Gretton, A. Demystifying mmd gans. *arXiv preprint arXiv:1801.01401*, 2018.
- Boys, B., Girolami, M., Pidstrigach, J., Reich, S., Mosca, A., and Akyildiz, O. D. Tweedie moment projected diffusions for inverse problems. *arXiv preprint arXiv:2310.06721*, 2023.
- Chen, T., Gu, J., Dinh, L., Theodorou, E., Susskind, J. M., and Zhai, S. Generative modeling with phase stochastic bridge. In *The Twelfth International Conference on Learning Representations*, 2024. URL <https://openreview.net/forum?id=tUtGjQEDd4>.
- Chung, H., Kim, J., Mccann, M. T., Klasky, M. L., and Ye, J. C. Diffusion posterior sampling for general noisy inverse problems. In *The Eleventh International Conference on Learning Representations*, 2022a.
- Chung, H., Sim, B., and Ye, J. C. Come-closer-diffuse-faster: Accelerating conditional diffusion models for inverse problems through stochastic contraction. In *Proceedings of the IEEE/CVF Conference on Computer Vision and Pattern Recognition*, pp. 12413–12422, 2022b.
- Daras, G., Chung, H., Lai, C.-H., Mitsufuji, Y., Ye, J. C., Milanfar, P., Dimakis, A. G., and Delbracio, M. A survey on diffusion models for inverse problems, 2024. URL <https://arxiv.org/abs/2410.00083>.
- Deng, J., Dong, W., Socher, R., Li, L.-J., Li, K., and Fei-Fei, L. Imagenet: A large-scale hierarchical image database. In *2009 IEEE conference on computer vision and pattern recognition*, pp. 248–255. Ieee, 2009.
- Dhariwal, P. and Nichol, A. Diffusion models beat gans on image synthesis. *Advances in neural information processing systems*, 34:8780–8794, 2021.
- Efron, B. Tweedie’s formula and selection bias. *Journal of the American Statistical Association*, 106:1602–1614, 12 2011. doi: 10.1198/jasa.2011.tm11181.
- Heusel, M., Ramsauer, H., Unterthiner, T., Nessler, B., and Hochreiter, S. Gans trained by a two time-scale update rule converge to a local nash equilibrium. *Advances in neural information processing systems*, 30, 2017.
- Ho, J. and Salimans, T. Classifier-free diffusion guidance. In *NeurIPS 2021 Workshop on Deep Generative Models and Downstream Applications*, 2021.
- Ho, J., Jain, A., and Abbeel, P. Denoising diffusion probabilistic models. *Advances in Neural Information Processing Systems*, 33:6840–6851, 2020.
- Holderrieth, P., Havasi, M., Yim, J., Shaul, N., Gat, I., Jaakkola, T., Karrer, B., Chen, R. T. Q., and Lipman, Y. Generator matching: Generative modeling with arbitrary markov processes, 2024. URL <https://arxiv.org/abs/2410.20587>.
- Huang, Y., Ghatore, A., Liu, Y., Hu, Z., Zhang, Q., Sastry, C. S., Gururani, S., Oore, S., and Yue, Y. Symbolic music generation with non-differentiable rule guided diffusion. In *ICML*, 2024. URL <https://openreview.net/forum?id=g8AigOTNXL>.
- Hyvärinen, A. and Dayan, P. Estimation of non-normalized statistical models by score matching. *Journal of Machine Learning Research*, 6(4), 2005.
- Kappen, H. Stochastic optimal control theory. *ICML, Helsinki, Radboud University, Nijmegen, Netherlands*, 2008.

- Kappen, H. J. Path integrals and symmetry breaking for optimal control theory. *Journal of Statistical Mechanics: Theory and Experiment*, 2005(11):P11011–P11011, November 2005. ISSN 1742-5468. doi: 10.1088/1742-5468/2005/11/p11011. URL <http://dx.doi.org/10.1088/1742-5468/2005/11/P11011>.
- Kappen, H. J., Gómez, V., and Opper, M. Optimal control as a graphical model inference problem. *Machine Learning*, 87(2):159–182, February 2012. ISSN 1573-0565. doi: 10.1007/s10994-012-5278-7. URL <http://dx.doi.org/10.1007/s10994-012-5278-7>.
- Karras, T. A style-based generator architecture for generative adversarial networks. *arXiv preprint arXiv:1812.04948*, 2019.
- Karras, T., Laine, S., and Aila, T. A Style-Based Generator Architecture for Generative Adversarial Networks. *IEEE Transactions on Pattern Analysis & Machine Intelligence*, 43(12):4217–4228, December 2021. ISSN 1939-3539. doi: 10.1109/TPAMI.2020.2970919. URL <https://doi.ieeecomputersociety.org/10.1109/TPAMI.2020.2970919>.
- Karras, T., Aittala, M., Aila, T., and Laine, S. Elucidating the design space of diffusion-based generative models. *Advances in Neural Information Processing Systems*, 35: 26565–26577, 2022.
- Kawar, B., Elad, M., Ermon, S., and Song, J. Denoising diffusion restoration models. *Advances in Neural Information Processing Systems*, 35:23593–23606, 2022.
- Kingma, D. P. and Ba, J. Adam: A method for stochastic optimization, 2017. URL <https://arxiv.org/abs/1412.6980>.
- Levine, S. Reinforcement learning and control as probabilistic inference: Tutorial and review, 2018. URL <https://arxiv.org/abs/1805.00909>.
- Li, A., Boyd, A., Smyth, P., and Mandt, S. Detecting and adapting to irregular distribution shifts in bayesian online learning. *Advances in neural information processing systems*, 34:6816–6828, 2021.
- Lipman, Y., Chen, R. T. Q., Ben-Hamu, H., Nickel, M., and Le, M. Flow matching for generative modeling. In *International Conference on Learning Representations*, 2023. URL <https://openreview.net/forum?id=PqvMRDCJT9t>.
- Liu, X., Gong, C., and qiang liu. Flow straight and fast: Learning to generate and transfer data with rectified flow. In *The Eleventh International Conference on Learning Representations*, 2023. URL <https://openreview.net/forum?id=XVjTT1nw5z>.
- Mardani, M., Song, J., Kautz, J., and Vahdat, A. A variational perspective on solving inverse problems with diffusion models. In *The Twelfth International Conference on Learning Representations*, 2023a.
- Mardani, M., Song, J., Kautz, J., and Vahdat, A. A variational perspective on solving inverse problems with diffusion models. *arXiv preprint arXiv:2305.04391*, 2023b.
- Nachmani, E., Roman, R. S., and Wolf, L. Denoising diffusion gamma models, 2021. URL <https://arxiv.org/abs/2110.05948>.
- Pandey, K., Pathak, J., Xu, Y., Mandt, S., Pritchard, M., Vahdat, A., and Mardani, M. Heavy-tailed diffusion models, 2024a. URL <https://arxiv.org/abs/2410.14171>.
- Pandey, K., Yang, R., and Mandt, S. Fast samplers for inverse problems in iterative refinement models. In *The Thirty-eighth Annual Conference on Neural Information Processing Systems*, 2024b. URL <https://openreview.net/forum?id=qxS4IvtLdD>.
- Podell, D., English, Z., Lacey, K., Blattmann, A., Dockhorn, T., Müller, J., Penna, J., and Rombach, R. SDXL: Improving latent diffusion models for high-resolution image synthesis. In *The Twelfth International Conference on Learning Representations*, 2024. URL <https://openreview.net/forum?id=di5zR8xgf>.
- Pokle, A., Muckley, M. J., Chen, R. T. Q., and Karrer, B. Training-free linear image inverses via flows. *Transactions on Machine Learning Research*, 2024. ISSN 2835-8856. URL <https://openreview.net/forum?id=PLIt3a4yTm>.
- Rombach, R., Blattmann, A., Lorenz, D., Esser, P., and Ommer, B. High-resolution image synthesis with latent diffusion models. In *Proceedings of the IEEE/CVF conference on computer vision and pattern recognition*, pp. 10684–10695, 2022.
- Rout, L., Chen, Y., Ruiz, N., Kumar, A., Caramanis, C., Shakkottai, S., and Chu, W.-S. Rb-modulation: Training-free personalization of diffusion models using stochastic optimal control, 2024. URL <https://arxiv.org/abs/2405.17401>.
- Saharia, C., Chan, W., Chang, H., Lee, C., Ho, J., Salimans, T., Fleet, D., and Norouzi, M. Palette: Image-to-image diffusion models. In *ACM SIGGRAPH 2022 conference proceedings*, pp. 1–10, 2022.
- Sohl-Dickstein, J., Weiss, E., Maheswaranathan, N., and Ganguli, S. Deep unsupervised learning using nonequilibrium thermodynamics. In *International Conference on Machine Learning*, pp. 2256–2265. PMLR, 2015.

- Song, J., Meng, C., and Ermon, S. Denoising diffusion implicit models, 2022a. URL <https://arxiv.org/abs/2010.02502>.
- Song, J., Vahdat, A., Mardani, M., and Kautz, J. Pseudoinverse-guided diffusion models for inverse problems. In *International Conference on Learning Representations*, 2022b.
- Song, Y. and Ermon, S. Generative modeling by estimating gradients of the data distribution. *Advances in neural information processing systems*, 32, 2019.
- Song, Y., Sohl-Dickstein, J., Kingma, D. P., Kumar, A., Ermon, S., and Poole, B. Score-based generative modeling through stochastic differential equations. In *International Conference on Learning Representations*, 2020.
- Song, Y., Durkan, C., Murray, I., and Ermon, S. Maximum likelihood training of score-based diffusion models. In Beygelzimer, A., Dauphin, Y., Liang, P., and Vaughan, J. W. (eds.), *Advances in Neural Information Processing Systems*, 2021. URL <https://openreview.net/forum?id=AklttWFnxS9>.
- Tran, P., Tran, A. T., Phung, Q., and Hoai, M. Explore image deblurring via encoded blur kernel space. In *Proceedings of the IEEE/CVF Conference on Computer Vision and Pattern Recognition (CVPR)*, pp. 11956–11965, June 2021.
- Vincent, P. A connection between score matching and denoising autoencoders. *Neural computation*, 23(7):1661–1674, 2011.
- Wang, H., Zhang, X., Li, T., Wan, Y., Chen, T., and Sun, J. Dmplug: A plug-in method for solving inverse problems with diffusion models, 2024. URL <https://arxiv.org/abs/2405.16749>.
- Yu, J., Wang, Y., Zhao, C., Ghanem, B., and Zhang, J. Freedom: Training-free energy-guided conditional diffusion model. In *Proceedings of the IEEE/CVF International Conference on Computer Vision (ICCV)*, pp. 23174–23184, October 2023.
- Zhang, C., Bütepage, J., Kjellström, H., and Mandt, S. Advances in variational inference. *IEEE transactions on pattern analysis and machine intelligence*, 41(8):2008–2026, 2018a.
- Zhang, R., Isola, P., Efros, A. A., Shechtman, E., and Wang, O. The unreasonable effectiveness of deep features as a perceptual metric. In *Proceedings of the IEEE conference on computer vision and pattern recognition*, pp. 586–595, 2018b.
- Zhou, M., Chen, T., Wang, Z., and Zheng, H. Beta diffusion, 2023. URL <https://arxiv.org/abs/2309.07867>.

A. Proofs

A.1. Simplification of the NDTM Objective for DDIM

We restate the theoretical result for convenience.

Proposition A.1. *For the diffusion posterior parameterization in Song et al. (2022a), the objective in Eq. 16 can be simplified as (see proof in Appendix A.1),*

$$\mathcal{C} \leq \kappa_t^2 \|\mathbf{u}_t\|_2^2 + \tau_t^2 \|\epsilon_\theta(\bar{\mathbf{x}}_t, t) - \epsilon_\theta(\mathbf{x}_t, t)\|_2^2 + w_T \Phi(\hat{\mathbf{x}}_0^t). \quad (20)$$

where $\bar{\mathbf{x}}_t = \mathbf{x}_t + \gamma \mathbf{u}_t$ is the guided state and the coefficients $\kappa_t = \frac{\gamma \sqrt{\alpha_{t-1}}}{\sqrt{\alpha_t}}$ and $\tau_t = \sqrt{1 - \alpha_{t-1} - \sigma_t^2} - \frac{\sqrt{\alpha_{t-1}(1 - \alpha_t)}}{\sqrt{\alpha_t}}$ are time-dependent scalars.

Proof. In the case of DDIM (Song et al., 2022a), the diffusion posterior is parameterized as (Eqn. 12 in Song et al. (2022a)),

$$\boldsymbol{\mu}_\theta(\mathbf{x}_t, t) = \frac{\sqrt{\alpha_{t-1}}}{\sqrt{\alpha_t}} \mathbf{x}_t + \underbrace{\left[\sqrt{1 - \alpha_{t-1} - \sigma_t^2} - \frac{\sqrt{\alpha_{t-1}(1 - \alpha_t)}}{\sqrt{\alpha_t}} \right]}_{=\tau_t} \epsilon_\theta(\mathbf{x}_t, t). \quad (21)$$

where the diffusion noising process is parameterized as $p(\mathbf{x}_t | \mathbf{x}_0) = \mathcal{N}(\sqrt{\alpha_t} \mathbf{x}_0, (1 - \alpha_t) \mathbf{I}_d)$ and $\epsilon_\theta(\mathbf{x}_t, t)$ is a pretrained denoiser which models $\mathbb{E}[\epsilon | \mathbf{x}_t]$ and intuitively predicts the amount of noise added to \mathbf{x}_0 for a given noisy state \mathbf{x}_t at time t . Additionally, for notational convenience, we denote the coefficient of the denoiser in Eq. 21 as τ_t . Following Song et al. (2022a), the coefficient σ is further defined as,

$$\sigma_t = \sqrt{\frac{(1 - \alpha_{t-1})}{(1 - \alpha_t)} \left(1 - \frac{\alpha_t}{\alpha_{t-1}}\right)} \quad (22)$$

It follows that,

$$\boldsymbol{\mu}_\theta(\mathbf{x}_t, t) = \frac{\sqrt{\alpha_{t-1}}}{\sqrt{\alpha_t}} \mathbf{x}_t + \tau_t \epsilon_\theta(\mathbf{x}_t, t) \quad (23)$$

$$\boldsymbol{\mu}_\theta(\mathbf{x}_t + \gamma \mathbf{u}_t, t) = \frac{\sqrt{\alpha_{t-1}}}{\sqrt{\alpha_t}} (\mathbf{x}_t + \gamma \mathbf{u}_t) + \tau_t \epsilon_\theta(\mathbf{x}_t + \gamma \mathbf{u}_t, t) \quad (24)$$

$$= \frac{\sqrt{\alpha_{t-1}}}{\sqrt{\alpha_t}} \mathbf{x}_t + \underbrace{\frac{\gamma \sqrt{\alpha_{t-1}}}{\sqrt{\alpha_t}} \mathbf{u}_t}_{=\kappa_t} + \tau_t \epsilon_\theta(\mathbf{x}_t + \gamma \mathbf{u}_t, t) \quad (25)$$

where we denote the coefficient of the control signal \mathbf{u}_t in the above equation as κ_t for notational convenience. Consequently, the NDTM cost in Eq. 16 can be simplified for the DDIM posterior parameterization in Eq. 21 as,

$$\mathcal{C} = \left[\|\boldsymbol{\mu}_\theta(\mathbf{x}_t + \gamma \mathbf{u}_t, t) - \boldsymbol{\mu}_\theta(\mathbf{x}_t, t)\|_2^2 + w_T \Phi(\hat{\mathbf{x}}_0^t) \right] \quad (26)$$

$$= \left[\|\kappa_t \mathbf{u}_t + \tau_t (\epsilon_\theta(\mathbf{x}_t + \gamma \mathbf{u}_t, t) - \epsilon_\theta(\mathbf{x}_t, t))\|_2^2 + w_T \Phi(\hat{\mathbf{x}}_0^t) \right] \quad (27)$$

$$\stackrel{(i)}{\leq} \kappa_t^2 \|\mathbf{u}_t\|_2^2 + \tau_t^2 \|\epsilon_\theta(\mathbf{x}_t + \gamma \mathbf{u}_t, t) - \epsilon_\theta(\mathbf{x}_t, t)\|_2^2 + w_T \Phi(\hat{\mathbf{x}}_0^t) \quad (28)$$

where (i) follows from the triangle inequality. This completes the proof. \square

A.2. Continuous-Time Diffusion Trajectory Matching

Analogous to the discrete case, we represent unguided diffusion dynamics using the following continuous-time reverse diffusion dynamics (Anderson, 1982; Song et al., 2020),

$$d\mathbf{x}_t = \left[f(t) \mathbf{x}_t - g(t)^2 \mathbf{s}_\theta(\mathbf{x}_t, t) \right] dt + g(t) d\mathbf{w}_t, \quad (29)$$

where $s_\theta(\mathbf{x}_t, t)$ is a pretrained score network. Similarly, we parameterize the *guided* continuous dynamics by inserting the control non-linearly into the score function follows,

$$d\mathbf{x}_t = \left[f(t)\mathbf{x}_t - g(t)^2 \mathbf{s}_\theta(\mathbf{x}_t, \mathbf{u}_t, t) \right] dt + g(t)d\mathbf{w}_t. \quad (30)$$

Denote the unguided path measure as $\mathbf{u}(\mathbf{x}(T \rightarrow 0))$ and the guided path measure as $\mu(\mathbf{x}(T \rightarrow 0)|\mathbf{u}(T \rightarrow 0))$.

Then, the optimal control problem reads, in analogy to Eq. (8):

$$\mathcal{C}(\mathbf{x}_T, \mathbf{u}(T \rightarrow 0)) = w_T \underbrace{\mathbb{E}_\mu[\Phi(\mathbf{x}_0)]}_{\text{Terminal Cost } \mathcal{C}_e} + \underbrace{D_{\text{KL}}(\mu(x(T \rightarrow 0)|\mathbf{x}_T, \mathbf{u}(T \rightarrow 0)) \parallel \nu(x(T \rightarrow 0)|\mathbf{x}_T))}_{\text{Transient Cost } \mathcal{C}_r}. \quad (31)$$

By (Song et al., 2021, Theorem 1 in Appendix A) (which follows from an application of Girsanov’s Theorem), the transient cost reads:

$$\mathcal{C}_r = D_{\text{KL}}(\mu(x(T \rightarrow 0)|\mathbf{x}_T, \mathbf{u}(T \rightarrow 0)) \parallel \nu(x(T \rightarrow 0)|\mathbf{x}_T)) \quad (32)$$

$$= \frac{1}{2} \int g(t)^2 \mathbb{E}_\mu \|\mathbf{s}_\theta(\mathbf{x}_t, \mathbf{u}_t, t) - \mathbf{s}_\theta(\mathbf{x}_t, t)\|^2 dt. \quad (33)$$

Taking the approximation that the control signal is optimized greedily, we find Eq. (12).

A.3. Extension to Flow Matching Models

For continuous flow matching models (Lipman et al., 2023; Albergo & Vanden-Eijnden, 2023; Liu et al., 2023) with a vector field $\mathbf{v}_\theta(\mathbf{x}_t, t)$,

$$d\mathbf{x}_t = \mathbf{v}_\theta(\mathbf{x}_t, t)dt, \quad (34)$$

we insert the control signal into the dynamics through an additional dependence of the velocity field:

$$\frac{d\mathbf{x}_t}{dt} = \mathbf{v}_\theta(\mathbf{x}_t, \mathbf{u}_t, t). \quad (35)$$

Since flow matching uses the squared loss, it is natural to regularize deviation from the unguided trajectory in terms of the velocity field:

$$\mathcal{C}_r = \int \|\mathbf{v}_\theta(\mathbf{x}_t, \mathbf{u}_t, t) - \mathbf{v}_\theta(\mathbf{x}_t, t)\|^2 dt \quad (36)$$

B. Implementation Details

In this section, we include practical implementation details for the results presented in Section 4.

B.1. Task Details

Here, we describe the task setup in more detail.

Superresolution (x4): We follow the setup from DPS (Chung et al., 2022a), More specifically,

$$\mathbf{y} \sim \mathcal{N}(\mathbf{y} | \mathbf{L}^f \mathbf{x}, \sigma_y^2 \mathbf{I}), \quad (37)$$

where \mathbf{L}^f represents the bicubic downsampling matrix with downsampling factor f . In this work, we fix f to 4 for both datasets.

Random Inpainting (90%) We use random inpainting with a dropout probability of 0.9 (or 90%). For this task, the forward model can be specified as,

$$\mathbf{y} \sim \mathcal{N}(\mathbf{y} | \mathbf{M}\mathbf{x}, \sigma_y^2 \mathbf{I}_d) \quad (38)$$

where $\mathbf{M} \in \{0, 1\}^{d \times d}$ is the masking matrix.

Non-Linear Deblurring We use the non-linear deblurring setup from DPS. More specifically, we use the forward operator \mathcal{F}_ϕ (modeled using a neural network) for the non-linear deblurring operation. Given pairs of blurred and sharp images, $\{\mathbf{x}_i, \mathbf{y}_i\}$, one can train a forward model estimator as (Tran et al., 2021),

$$\phi^* = \arg \min_{\phi} \|\mathbf{y}_i - \mathcal{F}_\phi(\mathbf{x}_i, \mathcal{G}_\phi(\mathbf{x}_i, \mathbf{y}_i))\|_2^2 \quad (39)$$

where \mathcal{G} extracts the kernel information from the training pairs. At inference, the operator \mathcal{G} can instead be replaced by a Gaussian random vector \mathbf{g} . In this case, the inverse problem reduces to recovering \mathbf{x}_i from \mathbf{y}_i . In this work, we directly adopt the default settings from DPS.

Blind Image Deblurring (BID) We directly adopt the setup for blind image deblurring from DMPlug (see Appendix C.4 in Wang et al. (2024) for more details). More specifically, in the BID task, the goal is to recover the kernel \mathbf{k} in addition to the original signal \mathbf{x}_0 such that,

$$\mathbf{y} = \mathbf{k} * \mathbf{x}_0 + \sigma_y \mathbf{z} \quad (40)$$

In this work, we adapt the default settings from DMPlug. For BID (Gaussian), the kernel size is 64×64 with the standard deviation set to 3.0. For BID (Motion), the kernel intensity is adjusted to 0.5.

B.2. Task Specific Hyperparameters

Here, we provide a detailed overview of different hyperparameters for the baselines considered in this work. We optimize all baselines and our method for the best sample perceptual quality. We use the official code implementation for RED-Diff (Mardani et al., 2023a) at <https://github.com/NVlabs/RED-diff>, <https://github.com/mandt-lab/c-pigdm> and <https://github.com/sun-umn/DMPlug> for running all competing baselines.

B.2.1. DPS (CHUNG ET AL., 2022A)

We adopt the DPS parameters from Mardani et al. (2023a). More specifically, we fix the number of diffusion steps to 1000 using the DDIM sampler. We set $\eta = 0.5$ for all tasks. Following Chung et al. (2022a), we set,

$$\zeta = \frac{\alpha}{\|\mathbf{y} - \mathcal{A}(\hat{\mathbf{x}}_0)\|_2^2} \quad (41)$$

Table 4 illustrates different hyperparams for DPS on all tasks for the FFHQ and ImageNet datasets.

B.2.2. DDRM (KAWAR ET AL., 2022)

Following Kawar et al. (2022), we fix $\eta = 0.85$, $\eta_b = 1.0$, and the number of diffusion steps to 20 across all linear inverse problems.

B.2.3. C-IIGDM (PANDEY ET AL., 2024B)

We set the number of diffusion steps to 20 for all tasks. It is also common to contract the reverse diffusion sampling for better sample quality by initializing the noisy state as proposed in Chung et al. (2022b). We denote the start time as τ . We re-tune C-IIGDM for the best perceptual quality for all linear inverse problems. Table 5 illustrates different hyperparams for linear inverse problems. We find that C-IIGDM fails to recover plausible images for random inpainting task after numerous tuning attempts.

B.2.4. RED-DIFF (MARDANI ET AL., 2023A)

We set $\sigma_0 = 0$ with a linear weighting schedule and $lr = 0.5$, $\lambda = 0.25$ and perform 50 diffusion steps for all tasks across the FFHQ and ImageNet dataset. We highlight different hyperparams in Table 6.

B.2.5. NDTM (OURS)

We use the Adam optimizer (Kingma & Ba, 2017) with default hyperparameters, fixing the learning rate to 0.01 for updating the control \mathbf{u}_t across all tasks and fix the kernel learning rate in the BID task to 0.01. We refer to the loss weighting scheme in Eq. 16 as "DDIM weighting". Moreover, we use linear decay for the learning rate. We perform 50 diffusion steps across

Table 4. DPS hyperparameters used for different tasks

Task	FFHQ	ImageNet
	α	α
Super-Resolution (4x)	1.0	1.0
Random Inpainting (90%)	1.0	1.0
Non-Linear Deblur	0.3	1.0

Table 5. C-IIGDM hyperparameters used for different tasks. We find that C-IIGDM fails to recover plausible images for this task after numerous tuning attempts.

Task	FFHQ			ImageNet		
	λ	w	τ	α	w	τ
Super-Resolution (4x)	-0.4	4.0	0.4	-0.4	4.0	0.4
Random Inpainting (90%)	-	-	-	-	-	-

Table 6. RED-Diff hyperparameters used for different tasks.

Task	FFHQ		ImageNet	
	lr	λ	lr	λ
Super-Resolution (4x)	0.5	1.0	0.5	0.4
Random Inpainting (90%)	0.5	0.25	0.5	0.25
Non-Linear Deblur	0.5	0.25	0.5	0.25

all datasets and tasks. We tune the guidance weight γ , the number of optimization steps N , loss weighting (w_T , w_{score} , w_{control}), DDIM η and the truncation time τ (Chung et al., 2022b) for best performance across different tasks. All these hyperparameters are listed in Table 8.

C. Additional Experimental Results

C.1. Evaluation on Distortion Metrics

In this work, we primarily optimize all competing methods for perceptual quality. However, for completeness, we compare the performance of our proposed method with other baselines on recovery metrics like PSNR and SSIM. Tables 11 and 12 compare our proposed method, NDTM, with competing baselines for linear and non-linear inverse problems. We find that NDTM performs on par with other methods for the super-resolution task. However, for random inpainting and non-linear deblur, NDTM outperforms competing methods in terms of distortion metrics like PSNR. Since NDTM also outperforms existing baselines in terms of perceptual quality (see Table 3), our method provides a better distortion-perception tradeoff.

C.2. Runtime

Below, we compare different methods in terms of the wall-clock time required for running on a single image for the superresolution task. From Table 9, we observe that while our method requires an inner optimization loop, it is still faster than common baselines like DPS and DMPlug (see Table 10).

Variational Control for Guidance in Diffusion Models

Table 7. BID hyperparameters for NDTM.

Task	FFHQ						
	N	γ_t	η	τ	w_T	w_{score}	$w_{control}$
BID (Gaussian)	15	1.0	0.7	1000	50	ddim	ddim
BID (Motion)	15	1.0	0.7	1000	50	ddim	ddim

Table 8. NDTM hyperparameters for different tasks.

Task	FFHQ							ImageNet						
	N	γ	η	τ	w_T	w_{score}	$w_{control}$	N	γ	η	τ	w_T	w_{score}	$w_{control}$
Super-Resolution (4x)	5	1.0	0.7	400	50	ddim	ddim	2	2.0	0.1	600	50	ddim	ddim
Random Inpainting (90%)	2	4.0	0.2	500	1	0	0	2	4.0	0.0	600	50	ddim	ddim
Non-Linear Deblur	5	5.0	0.1	400	1	0	0	2	4.0	0.1	600	50	ddim	ddim

Table 9. Runtime comparisons for different baselines vs NDTM for super-resolution task on both datasets. The runtime numbers are in wall-clock time (seconds) and tested on a single RTX A6000 GPU.

	FFHQ (256 × 256)					Imagenet (256 × 256)				
	DPS	RED-diff	C-IIGDM	DDRM	NDTM (Ours)	DPS	RED-diff	C-IIGDM	DDRM	NDTM (Ours)
Runtime (secs / Img)	199.1	5.8	3.68	1.3	13.6	399.3	7.1	16.4	2.4	38.3

Table 10. Runtime comparisons for DMPlug baseline vs NDTM for blind image deblurring (BID) task on FFHQ dataset. The runtime numbers are in wall-clock time (minutes) per image and tested on a single RTX A6000 GPU.

Method	Gaussian blur	Motion blur
	Time↓	Time↓
DMPlug	51.24	51.13
NDTM [†] (Ours)	7.17	7.17
NDTM [§] (Ours)	18.07	18.13

Table 11. Comparison between NDTM and existing methods for Linear IPs on distortion metrics like PSNR and SSIM. Missing entries indicate that the method was unstable for that specific task. **Bold**: best.

Method	Super-Resolution (4x)				Random Inpainting (90%)			
	FFHQ (256 × 256)		Imagenet (256 × 256)		FFHQ (256 × 256)		Imagenet (256 × 256)	
	PSNR↑	SSIM↑	PSNR↑	SSIM↑	PSNR↑	SSIM↑	PSNR↑	SSIM↑
DPS	29.06	0.832	23.61	0.676	27.76	0.832	20.96	0.657
DDRM	30.12	0.864	24.15	0.701	17.34	0.371	15.91	0.257
RED-diff	27.67	0.720	24.06	0.685	20.84	0.581	18.63	0.466
C-IIGDM	27.93	0.773	23.20	0.631	-	-	-	-
NDTM (ours)	29.06	0.833	23.12	0.674	28.03	0.834	21.34	0.665

Table 12. NDTM outperforms existing methods for Non-linear deblur on distortion metrics like PSNR and SSIM. **Bold**: best.

Method	FFHQ (256 × 256)		ImageNet (256 × 256)	
	PSNR↑	SSIM↑	PSNR↑	SSIM↑
DPS	8.12	0.262	6.67	0.156
RED-diff	24.88	0.717	21.88	0.623
NDTM (ours)	30.64	0.874	24.41	0.732



Figure 5. Qualitative comparison between NDTM and competing baselines on the Non-Linear Deblurring task. NDTM better recovers the structure of the image compared to other baselines. We find that DPS is unstable for this task often generating reconstructions with no information.

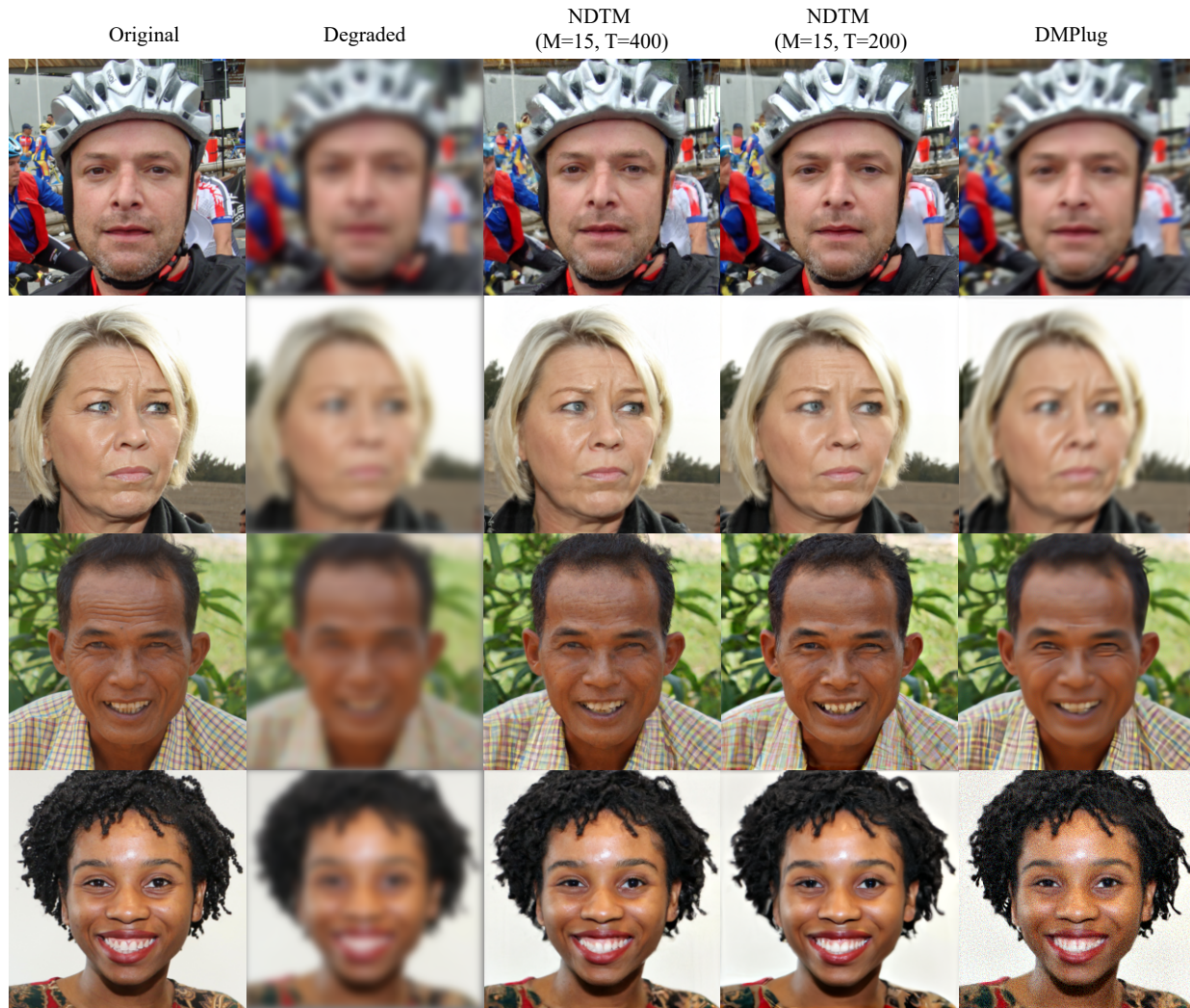


Figure 6. Qualitative comparison between NDTM and competing baseline (DMPlug) on the blind image deblurring task. NDTM better recovers the details and structure of the image compared to the baseline. We find DMPlug introduces noisy artifacts and blurry images in some samples.



Figure 7. Qualitative comparison between NDTM and competing baselines on the Random Inpainting (90%) Task. NDTM better recovers the structure of the image compared to other baselines.



Figure 8. Qualitative comparison between NDTM and competing baselines on 4x super-resolution task. NDTM better recovers the structure of the image compared to other baselines. Best viewed when zoomed in.